Published in final edited form as:
Anal Chem. 2010 November 15; 82(22): 9344–9349. doi:10.1021/ac1019123.

Achieving 50% ionization efficiency in sub-ambient pressure ionization with nanoelectrospray

Ioan Marginean, **Jason S. Page**, **Aleksey V. Tolmachev**, **Keqi Tang**, and **Richard D. Smith**[a]
Biological Sciences Division, Pacific Northwest National Laboratory, P.O. Box 999, Richland, Washington 99352

Abstract

Inefficient ionization and poor transmission of the charged species produced by an electrospray from the ambient pressure mass spectrometer source into the high vacuum region required for mass analysis significantly limits achievable sensitivity. Here we present evidence that, when operated at flow rates of 50 nL/min, a new electrospray-based ion source operated at ~20 Torr can deliver ~50% of the analyte ions initially in the solution as charged desolvated species into the rough vacuum region of mass spectrometers. The ion source can be tuned to optimize the analyte signal for readily ionized species while reducing the background contribution.

INTRODUCTION

The sensitivity of sample-limited analyses and the ability to detect low-concentration analytes are constrained by losses during sample preparation and analysis. Often, it is critical that the instrument used for analysis is optimized to reduce sample losses in order for low level species to be detected. For electrospray ionization-mass spectrometry (ESI-MS), analyte ions produced by an ESI source are conventionally transferred from a near ambient pressure region outside of the mass spectrometer to the high vacuum MS detector region required for mass-analysis. Generally some ion losses occur at every conductance limiting aperture, with the major losses by far at the atmospheric pressure ESI-MS interface. Early transmission measurements estimated that significantly less than 1% of the electrospray current was sampled from atmospheric pressure into the first vacuum stage of a mass spectrometer,1 with most of the charged aerosol lost to the front-end of the interface and inside the capillary inlet.2, 3 To increase the transmission efficiency, Schneider et al increased the inlet aperture to 0.88 mm dramatically reducing these losses;4 the higher gas load, however, required additional pumping (five pumps for the first vacuum stage alone), rendering this approach impractical.

The ion utilization efficiency under particular experimental conditions can be characterized by the ratio between the number of ions reaching the detector and the total number of ions in the solution delivered to the ionization source. It was recognized early that a larger fraction of ions can be detected when the electrospray was operated at extremely low flow rates,5, 6 and a trend showing sharply increasing ion utilization efficiency with decreasing flow rates is clearly established.7–15 El-Faramawy et al. showed that 12% of the ions originally present in the solution could reach the detector at flow rates below 1 nL/min.16

The complexity of the ion formation mechanism in ESI is partly responsible for the low ion utilization efficiencies. An electrospray operated in the cone-jet regime generates droplets with the initial diameter proportional to the relaxation length:17

[a]rds@pnl.gov.

$$r^*=(Q\varepsilon\varepsilon_0/\kappa)^{1/3} \quad (1)$$

where κ, Q, ε, and ε_0, stand for liquid conductivity, flow rate, permittivity and vacuum permittivity, respectively. The droplet with initial diameter d_0 shrinks to a diameter d due to solvent evaporation following a d-square kinetics:18

$$d^2=d_0^2-kt \quad (2)$$

In a diffusion-controlled regime under steady environmental conditions, the rate coefficient k for a mono-component, isolated droplet can be approximated as:18

$$k=8\frac{\kappa_T}{\rho_l c_p}\ln\left[1+\frac{c_p(T_\infty-T)}{\Delta H_v^0}\right] \quad (3)$$

where κ_T, ρ_l, c_p, ΔH_v^0, T_∞, and T, stand for liquid thermal conductivity, density, specific heat, latent heat of evaporation, environment and droplet surface temperature. Rayleigh suggested that isolated droplets holding the charge q will become unstable when their diameters reach the so-called Rayleigh charge limit:19

$$q^2=\pi^2\varepsilon_0\gamma d^3 \quad (4)$$

where γ is liquid surface tension. Cumulative evidence shows that Rayleigh's predictions were both phenomenologically20 and quantitatively21 correct. It is commonly accepted that – following a Rayleigh fission – the parent droplet looses a relatively large percentage of its charge (sometimes up to 40%) along with a relatively small percentage of its mass (sometimes undetectable).22 Both the parent and the progeny droplets resume the cycle of solvent evaporation and Rayleigh fission23 until the droplets shrink down to a diameter in the order of 10 nm. The gas phase ions are generated via either the ion evaporation mechanism – IEM24, 25 or charge residue mechanism – CRM.26 While the exact mechanism of gas phase ion formation from the charged droplet at its final state is still debated due to the lack of direct experimental observation, the general consensus is that CRM is most likely correct for large molecular ions, while IEM correctly describes the ionization mechanism for small ionic species. For intermediate species the situation remains less certain although it can be argued that the CRM more likely applies for a broad range of peptides as their behavior is both similar to that for larger proteins (where the CRM almost certainly applies), and there is no evidence for a shift in mechanism as a function of peptide size.

The formation of small droplets is a prerequisite for ion transfer into the gas phase by both IEM and CRM. Due to higher mobilities, the smaller droplets are dispersed radially toward the outskirt of the electrospray plume.27, 28 The first gas-phase ions most likely originate from surface active species associated with progeny droplets travelling away from the spray axis, while the ions remaining inside the larger droplets (more hydrophilic species for aqueous solutions) are transferred into the gas-phase later and downstream. Radial plume expansion and large differences in charge density and droplet sizes can disperse gas-phase ion creation to various locations and different times within the aerosol, creating challenges for the traditional approaches of ion sampling and transmission into the mass spectrometer. For example, a large percentage of the charged aerosol can be sampled into the mass

spectrometer when the ESI emitter is very close to the MS inlet, but incomplete ion desolvation limits MS sensitivity. If the emitter is moved a greater distance away from the inlet, most analyte ions should be in the gas phase, but the electrospray plume expansion precludes efficient ion collection.3

Assuming that all the analyte ions are transferred into the gas phase, the maximum achievable analyte current is:

$$I_{A,max} = n_A c_A Q F \quad (5)$$

where n_A, c_A, Q, and F stand for analyte charge, concentration, liquid flow rate, and Faraday's constant, respectively. Due to inefficiencies and losses analyte currents achieved in mass spectrometry are much smaller than $I_{A,max}$, and depends – among other experimental parameters – on emitter position in front of the ion inlet and the quality of the aerosol produced by the electrospray. The total electrospray current depends primarily on the solution surface tension, γ, conductivity, κ, permittivity, ε, and flow rate, Q as suggested by the scaling law:17

$$I_T \sim (\gamma Q \kappa / \varepsilon)^{1/2} \quad (6)$$

Because in most practical cases the solution conductivity is determined by its slight acidification, the two currents, $I_{A,max}$ and I_T, rarely correlate. To ensure effective analyte ion transfer into the gas phase, I_T should be several times larger than $I_{A,max}$; however, if I_T is too large, space-charge effects will increase radial expansion and may compromise the analyte ion transmission into the first vacuum stage of the mass spectrometer.29

A skimmer interface or other conductance limiting aperture is commonly employed to transfer the ions entering the first region from the atmospheric inlet into the next lower pressure region of a mass spectrometer. The size of the orifice is the result of a compromise between the desire for high ion transmission, the need to maintain the high vacuum required for mass analysis, and practical issues of pump size and cost. Ion funnels30 can improve the ion transmission in this region to almost 100% over useful m/z ranges with only modest pumping requirements.

Ion funnel technology has been used in our initial studies of sub-ambient pressure ionization with nanoelectrospray (SPIN).31 The SPIN source eliminates ion losses at the interface and inlet capillary as well as potential inlet biases against higher mobility species.32 However, ion production remains a challenge due to expected decrease in desolvation efficiency at reduced pressures. Here we present evidence that the SPIN source is able to achieve as much as 50% efficiency for the transfer of analyte species initially in the solution into the sub-Torr region of a mass spectrometer as gas-phase ions.

EXPERIMENTAL

Sample preparation

The ES solution was prepared by mixing purified water (Barnstead Nanopure Infinity System, Dubuque, IA, USA) and methanol (HPLC grade, Fisher Scientific, Fair Lawn, NJ, USA) in a 1:1 ratio, then adding acetic acid (Sigma–Aldrich, St. Louis, MO, USA) at 1% v/v. Neurotensin (Neu) stock solution was diluted in the ES solution to a final concentration of 3 μM unless otherwise noted.

ESI setup

ES emitters were manufactured by chemically etching sections of 10/150 μm i.d./o.d. fused silica tubing (Polymicro Technologies, Phoenix, AZ, USA).33 The distal end of the emitter was placed into the first vacuum region of the SPIN source via a PEEK bulkhead union and was connected to a transfer capillary through a stainless steel union. A Bertan 205B-03R high voltage power supply (Hicksville, NY) was connected to the stainless steel union to provide the ES voltage. The ES solution was loaded in 100 μL syringes (Hamilton, Las Vegas, NV) and continuously delivered to the ion source using a Harvard Apparatus model PHD 2000 syringe pump (Holliston, MA) at 200 nL/min, unless otherwise noted. Plugs of analyte dissolved in the same solvent were injected into the solvent flow using a manual 6-port valve (Valco Instruments Co., Houston, TX).

Instrumentation

The SPIN source design described in detail previously31 was slightly modified as depicted in Figure 1 to offer improved control over the ionization. MS and current measurements were performed with an Agilent MSD1100 (Agilent Technologies, Santa Clara, CA) single-quadrupole mass spectrometer equipped with a dual ion funnel (d, e, f) interface.34 Carbon dioxide was leaked inside the interface at a flow rate controlled by an Agilent G1995A flow meter. Addition of CO_2 dramatically improved the stability of the source by eliminating electric breakdown incidents. To improve the ionization efficiency, the gas was re-heated inside the brass chamber (a) immediately after its expansive cooling in the ~20 torr interface and guided around the ES emitter by the conical outlet with a 5-mm orifice (b). The gas temperature reached ~70°C for a chamber (a) temperature of 200°C. Losses to the cone were negligible due to the small spacing between the ES emitter and the orifice; even at larger spacing, they could be completely eliminated by an adequate CO_2 sheath gas flow rate. To measure the ion flux at the exit of the ion source, the transfer octopole following the low pressure ion funnel was biased at −3.1 V and used as current collector. These measurements will be referred to as current measurements, whereas the current measured by the MS detector will be referred to as ion current. The current was measured by floating a Keithley picoammeter to the biased voltage (Model 6485, Cleveland, OH) connected to a computer via a USB-6251 Multifunction Data Acquisition board (National Instruments, Austin, TX) to collect and analyze the data.

RESULTS AND DISCUSSION

The ion utilization efficiency is defined here as the ratio between the analyte ion current collected by the detector and the current theoretically expected if all analyte species are converted from the solution into gas phase ions ($I_{A,max}$). Similarly, ion source efficiency can be defined as the ratio between the analyte ion current exiting the ion source and $I_{A,max}$. We note that El-Faramawy et al.16 and Schneider et al.4 estimated the ion utilization efficiency of their interfaces based on the MS signal intensity and losses typically encountered in different sections of the mass spectrometer. To avoid detector-specific uncertainties, possible biases, assumptions in transmission efficiencies of the ion guiding components, and possible space charge bottlenecks downstream from the ion source, we characterized the ion source efficiency by measuring the ion current immediately after the low pressure ion funnel. This approach measures directly the efficiency of the ionization source and interface, rather than that of the mass spectrometer as a whole, enabling independent evaluation and tuning of the ion source for optimal performance.

Figure 2a shows a typical current measurement during the elution of a 3 μM neurotensin solution plug. If all neurotensin molecules in solution form 3+ charge state ions in the gas phase, the maximum expected analyte current would be $I_{A,max}$ = 2.89 nA, a relatively small

fraction of the total electrospray current, $I_T \approx 35–40$ nA. Before and after the analyte plug elution the dual ion funnel assembly transmitted only 160±4 pA (less than 1% of I_T), which was related to solvent clusters and impurities creating the background common to ESI mass spectra. The current increased significantly (by 418±13 pA) during the analyte plug elution. While this current rise was clearly related to the presence of the analyte in solution, the differences in current measurements do not fully account for the neurotensin ion contribution, as the background species also may change with the presence of the peptide and account for some portion of the observed difference. Possible reasons for the differences include the suppression of the background ions during analyte plug elution or the presence of contaminants in the analyte solution.

Understanding the nature of the ions transmitted by the dual ion funnel assembly is critical to correctly interpreting the data. Species with *m/z* below a certain threshold (determined e.g. by RF amplitudes and frequencies applied to the ion funnel35) are discriminated against and do not contribute to the measured current. The presence of the jet disruptor (Figure 1f) effectively prevents larger charged droplets from contributing to the transmitted current. Thus, the current exiting the source is carried by ions/clusters with *m/z* above the ion funnel transmission cut-off.

MS measurements were employed to clarify the nature of the ions contributing to the current measurements. Figure 2b shows a mass spectrum measured during the analyte plug elution. The Neu^{3+} peak is dominant during the analyte plug elution with another analyte peak, Neu^{2+}, present at less than 5% intensity. The black trace in Figure 2c is a mass spectrum corresponding to the ES solution ~1 minute after plug elution, while the cyan trace compares it with the spectrum provided in Figure 2b. Only a few unassigned peaks emerged during the analyte plug elution with intensities comparable to those of existing background peaks. The background baseline also increased by a factor of ~1.5; measurements in the 50–3000 *m/z* range (not shown) revealed a consistently larger background up to *m/z* = 1500.

Figure 2d shows the total ion current (TIC, cyan trace) overlapped with the background ion current (black trace), calculated by subtracting the intensity of the analyte-related peaks from the TIC. It was evident that the ion source efficiency could not be calculated solely based on the total current rise during the analyte plug elution captured by Figure 2. Although the current rise was mainly due to analyte ions, contributions from impurities and a slight increase in the baseline needed to be better understood. MS results deconvoluted the current rise, allowing for a reasonable estimate of analyte contribution, thus ion source efficiency.

Further experiments were performed by varying experimental parameters to explore the background and analyte contributions to the current rise during analyte plug elution, allowing a more accurate estimation of the ion source efficiency and to gain insight on ion formation in the subambient pressure environment.

Figure 3 compares current measurements and MS results as a function of the pressure in the high-pressure ion funnel chamber where the electrospray was operated. The open and solid squares represent the current due to solvent and the current rise during the analyte plug elution, respectively. To explore the make-up of the current detected on the octopole, MS measurements were then performed with the same experimental conditions. The open and solid circles represent the rise in TIC intensity of the background and the extracted ion intensity profile for the analyte-related signal, respectively. These results point to an optimum operating pressure of ~22 Torr, which represents a compromise between the optimum operating conditions for the ion funnel (lower pressure) and those ensuring optimum desolvation of electrospray droplets (higher pressure).

The sum of the MS intensities presented in Figure 3 as open and solid circles was proportional ($R^2 = 0.92$) with the ion current rise on the octopole during the analyte plug elution (solid squares). Thus, the MS measurements appear to provide a reasonably accurate estimate for the ion current makeup exiting the ion source. The background contribution to the current rise accompanying the analyte plug elution ranged between 15–25% with larger values corresponding to lower pressures. At the optimum pressure (~20–22 Torr), the contribution of the background to the current rise due to the analyte plug elution was less than 20%.

Figure 4 presents the effect of the CO_2 sheath gas flow rate as well as the high-pressure ion funnel RF confining voltage on current measurements using a 10μM neurotensin solution with the pressure inside the first vacuum chamber maintained at 22 Torr. The results can be explained by associating large and low gas flow rates with short and long residence times in the high-pressure ion funnel, where the desolvation and the ionization presumably occur. The analyte-related ion current (Figure 4a) showed a maximum at 0.4–0.6 L/min CO_2. The current decline at very low CO_2 flow rates was attributed to increased ion losses at the conical outlet (results not shown). The trends were consistent with the hypothesis of a bimodal droplet size distribution. At large CO_2 flow rates, where the residence time in the ion funnel is the shortest, the ionization occurs mostly from small droplets that can generate gas-phase ions early in the ionization process. Ions transferred into the gas phase from larger droplets start contributing to the current at larger residence times, enabled by lower CO_2 sheath gas flow rates.

Formation of background current (panel 4b) was also favored by low CO_2 flow rates; however, the solvent ion formation was less efficient at large gas flows and did not decline at very low gas flows. It is important to note that these results convolute the background ion formation with the transmission function of the ion funnel as operated which will provide a bias against low *m/z* species.36 The observed trends could be explained based upon expected biases analyte vs. solvent / background ions transfer into the gas phase. For example, more surface active, easy-to-ionize analytes, located at the surface of the initial electrospray droplets, should be incorporated preferentially into the small progeny droplets formed as a result of the downstream Rayleigh fission processes. The small droplets evaporate faster, leading to gas-phase ions earlier into the ionization process. Related effects and phenomena are still under investigation and will be the subject of a separate report. These observations may have useful practical applications, such as tuning of the ion source to optimize targeted analyte species, while minimizing ionization of background species.

As expected, the magnitude of the confining voltage was important for ion transfer. The ionization and ion collection efficiencies degraded significantly with decreasing confining voltage at high gas flows, while they were less affected by the confining voltage at lower gas flow presumably due to the less impinging gas flow on the ion funnel. The loss of droplets before generation of gas-phase ions could explain the experimental trends. Large gas flows appeared to increase such losses, while the ion funnel transmission was less affected at lower gas flows.

The effect of the gas flow rate on the analyte-related current suggests that most of the processes leading to gas phase ions take place inside the high-pressure ion funnel. Based on a 2-Torr difference between the pressure inside the electrospray chamber (b in Figure 1) and the pressure in the high-pressure ion funnel chamber (measured at a 2 L/min CO_2 flow rate), we estimated a linear velocity of the gas molecules at the conical outlet of ~100 m/s. This suggests a minimum of ~100 μs residence time inside the 10-cm high-pressure ion funnel, which offers an approximate time scale for the overall ionization process. Assuming a cone-jet electrospray operation at 200 nL/min, the initial droplet size can be estimated from (1) at

less than 200 nm. The kinetics of droplet evaporation and fission expressed by (2), (3) and (4) estimate that droplets of this size should completely evaporate in less than 2 μs. The discrepancy between the two time scales is due to model assumptions and differences with the present experimental conditions. For example, the model assumes an isolated droplet and steady, diffusion-controlled evaporation, conditions hardly met in an electrospray aerosol. Another assumption is that of sufficient heat to support the evaporation process, whereas the energy carried by the heated gas at 2 L/min would be sufficient to evaporate only ~50 nL/min solution.

Additional insight into the ion formation mechanism can be gained from Figure 5, which compares results obtained with solutions of 3 μM and 10 μM concentrations as a function of CO_2 flow rate. The current decline at low and high gas flow rates was already discussed; the following discussion will focus on the results at intermediate gas flow rates. Except for a slight increase with increasing residence time, the curve observed for 3 μM solutions showed little dependence on the gas flow rate; however, the 10 μM solution shows an increase at ~0.8 L/min flow rate. This difference between the curves at relatively low gas flows corresponds to analyte-related current originating from larger electrospray droplets, as discussed in the previous section. It was apparent that, when available in smaller concentration, the analyte was preferentially distributed inside the smaller droplets. When available at larger concentrations, the analyte would also populate larger droplets, which transfer ions into the gas phase at longer residence times, and consistent with the analyte partitioning model of Enke.37

Figure 6 shows the ion source efficiency as a function of pressure and liquid flow rate at a CO_2 flow rate of 1.6 L/min. As expected,[7–16, 29] the ion source efficiency increased with decreasing liquid flow rate. Accounting for the background rise during the analyte plug elution, the ion source efficiency reached 13%, 22%, and 49% at the optimum pressure for liquid flow rates of 200, 100, and 50 nL/min, respectively. These results emphasize the major role of liquid flow rate (and implicitly the initial droplet size) on ion utilization efficiency. Theoretically, the ion source efficiency should increase even more by reducing the flow rate below 50 nL/min; however, electrospray stability in sub-ambient pressure environment was insufficient for effective measurements at lower flow rates (note the larger error bars and the scatter in the data at the lowest flow rate reported, 50 nL/min). For comparison purposes, the ion utilization efficiency of 12% reported by El-Faramawy et al. at less than 1 nL/min[16] translates into ~30% ion source efficiency.[38] However we note the significantly higher efficiency in the present work was achieved at >50-fold greater flow rates and is much more suited for both robust operation and coupling with on-line separations, as well as of far greater analytical utility for measurements over a large dynamic range.

CONCLUSIONS

We characterized the electrospray ionization in a sub-ambient pressure environment to optimize the operating parameters so as to guide SPIN ion source refinement. The source operated optimally at pressures ~20 Torr, which provided the best compromise between efficient droplet desolvation and charged aerosol confinement in the ion funnel. The highest overall ion source efficiency (~50%) was achieved at the lowest liquid flow rate (~50 nL/min), but a rate still useful for coupling with on-line separations. Higher ion source efficiency without the losses specific to atmospheric pressure electrosprays may be achievable at even lower flow rates or by splitting the flow to an emitter array. The sheath gas flow rate provided a means for tuning the droplet residence time and potentially minimizing the ionization of background species. Longer residence times improved the ionization efficiency for both the analyte and other background/solvent species.

Acknowledgments

This research was supported by the NIH National Center for Research Resources (RR018522). Experimental portions were performed in the Environmental Molecular Sciences Laboratory, a DOE national scientific user facility located at the PNNL in Richland, Washington. PNNL is a multiprogram national laboratory operated by Battelle for the DOE under Contract DE-AC05-76RLO 1830.

REFERENCES

1. Smith RD, Loo JA, Edmonds CG, Barinaga CJ, Udseth HR. Anal. Chem. 1990; 62:882–899. [PubMed: 2194402]
2. Lin BW, Sunner J. J. Am. Soc. Mass Spectrom. 1994; 5:873–885.
3. Page JS, Kelly RT, Tang K, Smith RD. J. Am. Soc. Mass Spectrom. 2007; 18:1582–1590. [PubMed: 17627841]
4. Schneider BB, Javaheri H, Covey TR. Rapid Commun. Mass Spectrom. 2006; 20:1538–1544. [PubMed: 16628560]
5. Gale DC, Smith RD. Rapid Commun. Mass Spectrom. 1993; 7:1017–1021.
6. Wilm M, Mann M. Anal. Chem. 1996; 68:1–8. [PubMed: 8779426]
7. Davis MT, Stahl DC, Hefta SA, Lee TD. Anal. Chem. 1995; 67:4549–4556. [PubMed: 8633788]
8. Bateman KP, White RL, Thibault P. Rapid Commun. Mass Spectrom. 1997; 11:307–315.
9. Oosterkamp AJ, Gelpi E, Abian J. J. Mass Spectrom. 1998; 33:976–983. [PubMed: 9821328]
10. Alexander JN, Schultz GA, Poli JB. Rapid Commun. Mass Spectrom. 1998; 12:1187–1191.
11. Gucek M, Vreeken RJ, Verheij ER. Rapid Commun. Mass Spectrom. 1999; 13:612–619.
12. Geromanos S, Freckleton G, Tempst P. Anal. Chem. 2000; 72:777–790. [PubMed: 10701263]
13. Chang YZ, Chen YR, Her GR. Anal. Chem. 2001; 73:5083–5087. [PubMed: 11721903]
14. Bendahl L, Hansen SH, Olsen J. Rapid Commun. Mass Spectrom. 2002; 16:2333–2340. [PubMed: 12478579]
15. Ishihama Y, Katayama H, Asakawa N, Oda Y. Rapid Commun. Mass Spectrom. 2002; 16:913–918. [PubMed: 11968120]
16. El-Faramawy A, Siu KWM, Thomson BA. J. Am. Soc. Mass Spectrom. 2005; 16:1702–1707. [PubMed: 16095913]
17. Fernández de la Mora J, Loscertales IG. J. Fluid Mech. 1994; 260:155–184.
18. Rosner, DE. Transport Processes in Chemically Reacting Flow Systems. Butterworths; 1986.
19. Rayleigh L. Philosophical Magazine. 1882; 14:184–186.
20. Gomez A, Tang KQ. Phys. Fluids. 1994; 6:404–414.
21. Li KY, Tu HH, Ray AK. Langmuir. 2005; 21:3786–3794. [PubMed: 15835938]
22. Grimm RL, Beauchamp JL. Anal. Chem. 2002; 74:6291–6297. [PubMed: 12510751]
23. Doyle A, Moffett DR, Vonnegut B. Journal of Colloid Science. 1964; 19 136-&.
24. Iribarne JV, Thomson BA. J. Chem. Phys. 1976; 64:2287–2294.
25. Hogan CJ, Carroll JA, Rohrs HW, Biswas P, Gross ML. Anal. Chem. 2009; 81:369–377. [PubMed: 19117463]
26. Dole M, Mack LL, Hines RL, Mobley RC, Ferguson LD, Alice MB. J. Chem. Phys. 1968; 49:2240–2249.
27. Tang K, Gomez A. Phys. Fluids. 1994; 6:2317–2332.
28. Tang KQ, Smith RD. J. Am. Soc. Mass Spectrom. 2001; 12:343–347. [PubMed: 11281610]
29. Marginean I, Kelly RT, Prior DC, LaMarche BL, Tang KQ, Smith RD. Anal. Chem. 2008; 80:6573–6579. [PubMed: 18661954]
30. Kelly RT, Tolmachev AV, Page JS, Tang KQ, Smith RD. Mass Spectrom. Rev. 2010; 28:294–312. [PubMed: 19391099]
31. Page JS, Tang K, Kelly RT, Smith RD. Anal. Chem. 2008; 80:1800–1805. [PubMed: 18237189]
32. Page JS, Marginean I, Baker ES, Kelly RT, Tang KQ, Smith RD. J. Am. Soc. Mass Spectrom. 2009; 20:2265–2272. [PubMed: 19815425]

33. Kelly RT, Page JS, Luo QZ, Moore RJ, Orton DJ, Tang KQ, Smith RD. Anal. Chem. 2006; 78:7796–7801. [PubMed: 17105173]
34. Ibrahim Y, Tang KQ, Tolmachev AV, Shvartsburg AA, Smith RD. J. Am. Soc. Mass Spectrom. 2006; 17:1299–1305. [PubMed: 16839773]
35. Page JS, Tolmachev AV, Tang KQ, Smith RD. J. Am. Soc. Mass Spectrom. 2006; 17:586–592. [PubMed: 16503158]
36. Tolmachev AV, Kim T, Udseth HR, Smith RD, Bailey TH, Futrell JH. Int. J. Mass Spectrom. 2000; 203:31–47.
37. Enke CG. Anal. Chem. 1997; 69:4885–4893. [PubMed: 9406535]
38. Thomson, BA. Private communication. 2010.

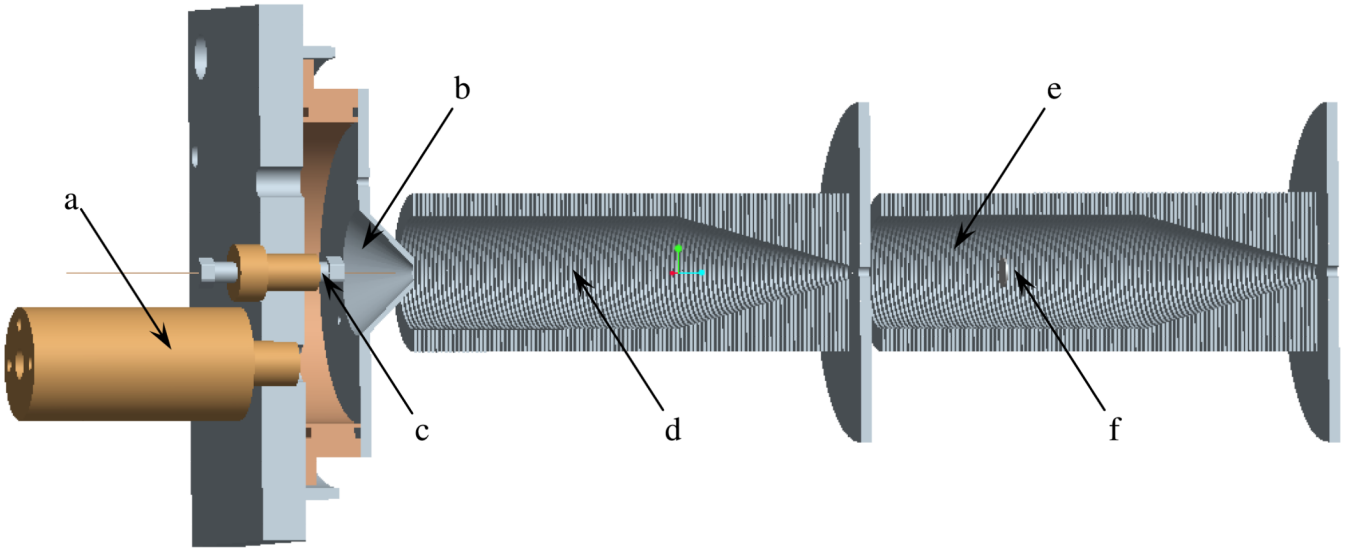

Figure 1.
Instrument configuration: (a) sheath gas heater chamber, (b) electrospray chamber with a 5-mm conical outlet, (c) emitter assembly, (d) high-pressure ion funnel, (e) low-pressure ion funnel, (f) jet disruptor.

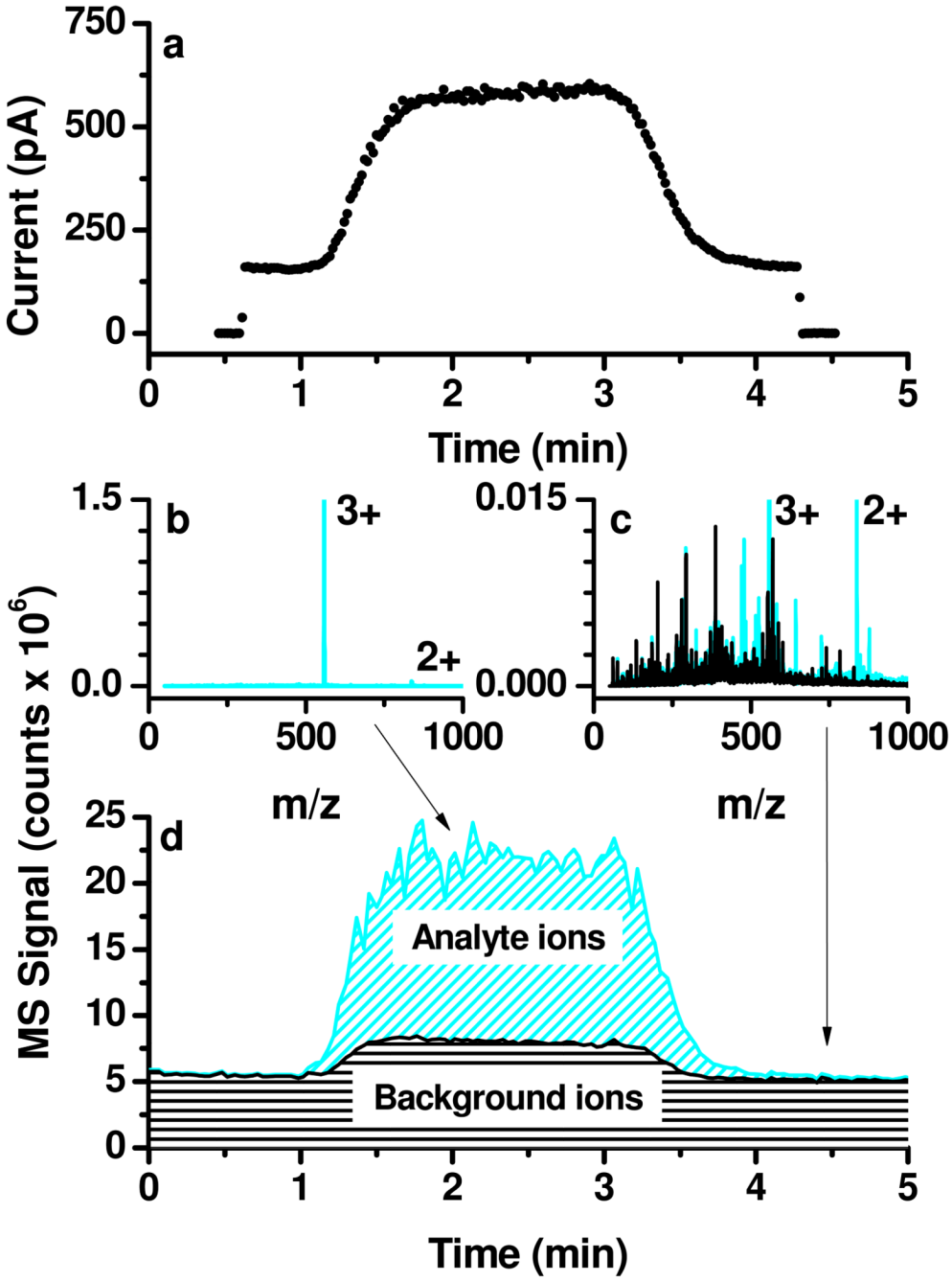

Figure 2.
Typical current and MS measurements during the analyte plug elution: (a) current collected on the octopole following transmission through the low-pressure ion funnel; (b) analyte and (c) solvent mass spectra; (d) total and background ion currents.

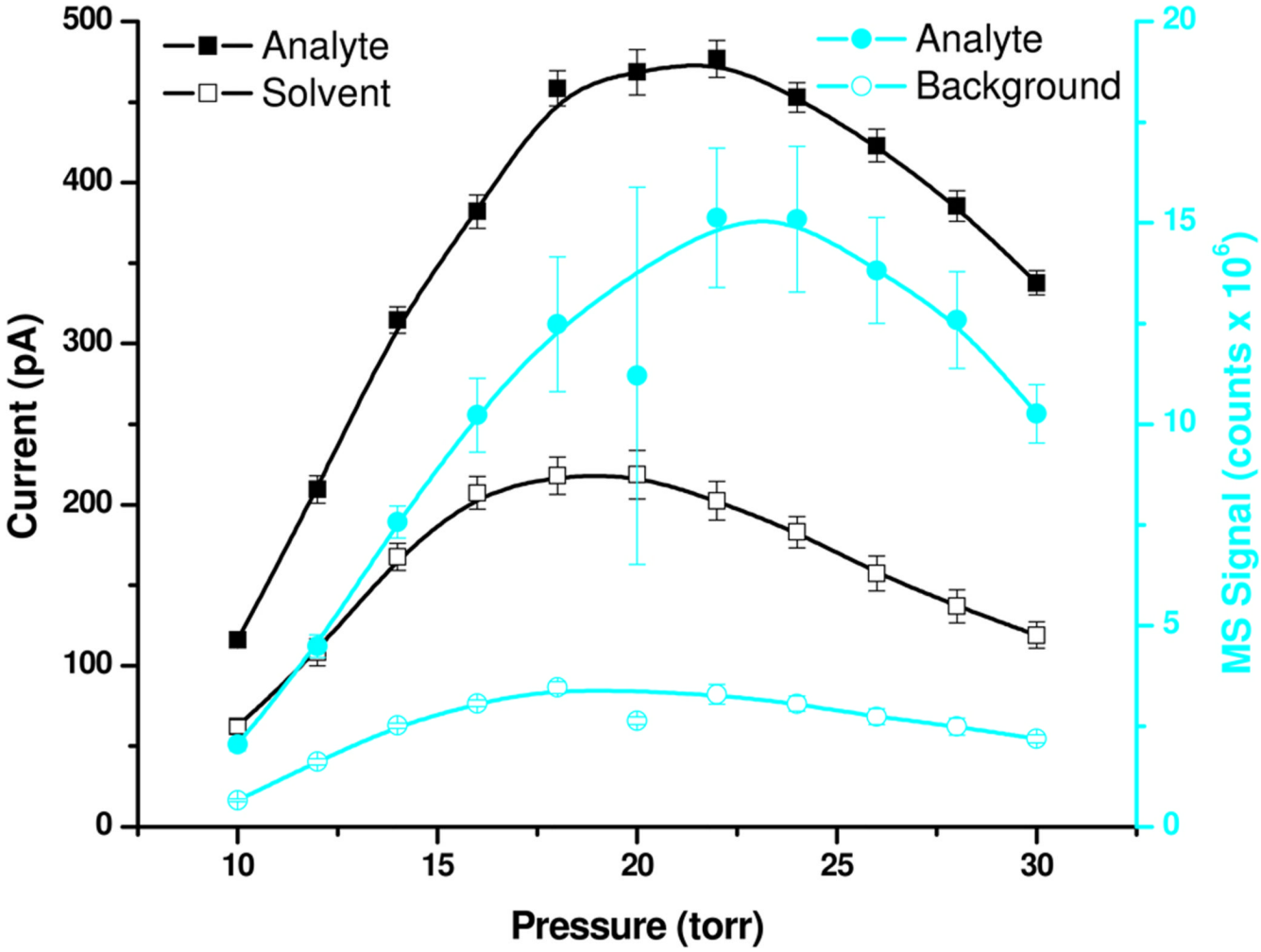

Figure 3.
Effect of pressure on current and MS signal.

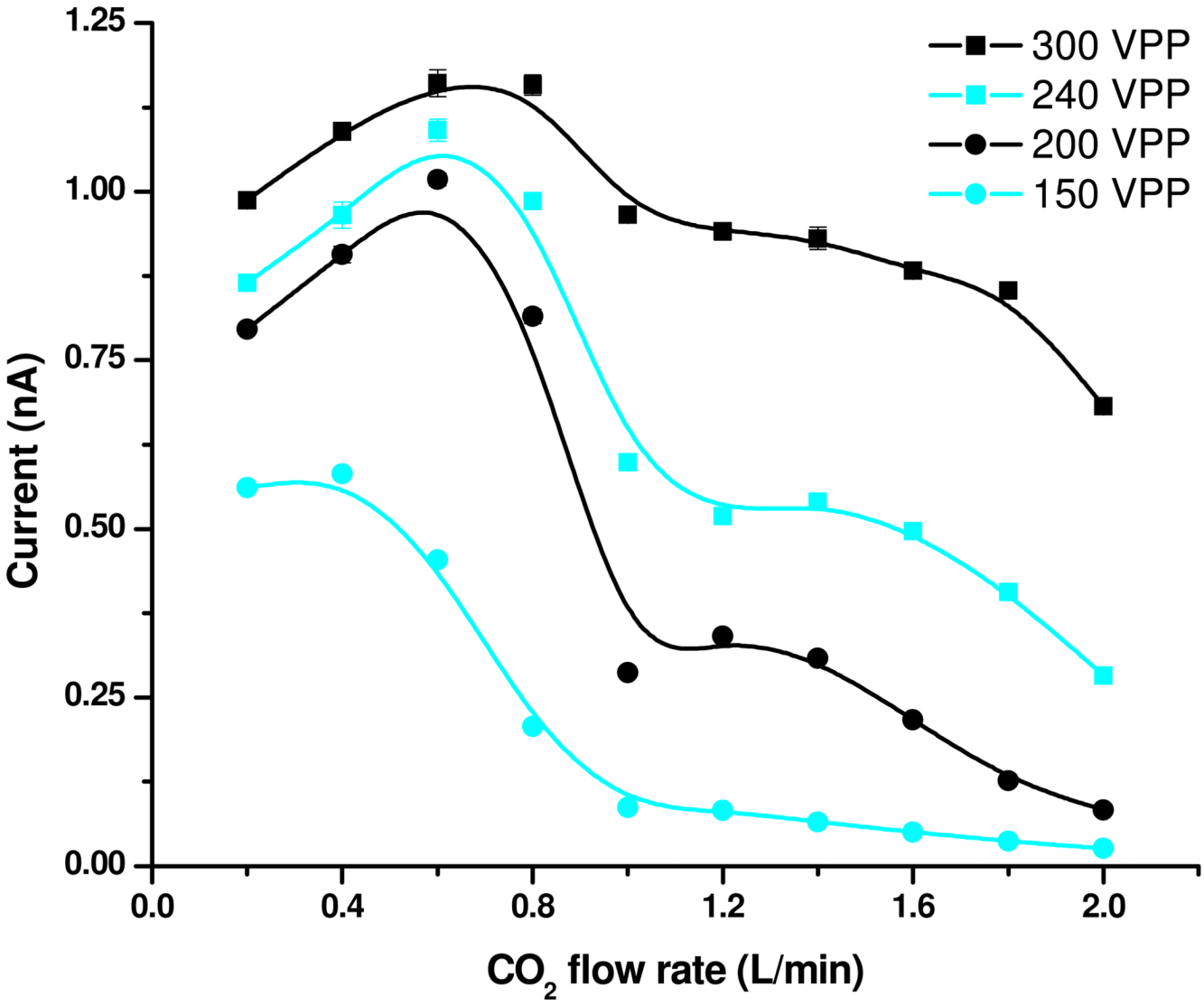

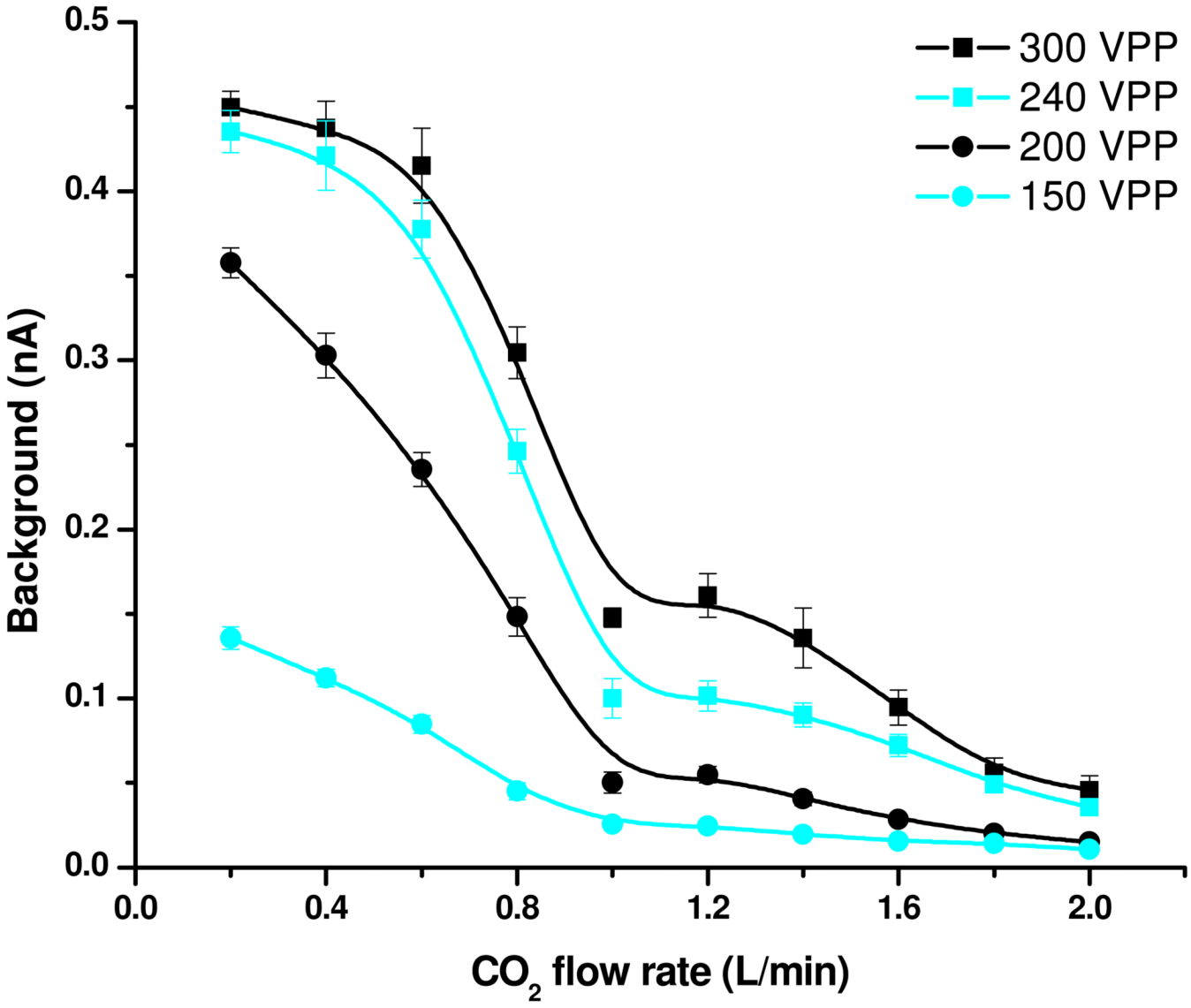

Figure 4.
Effect of RF confining voltage and CO_2 flow rate on (a) analyte-related and (b) solvent / background current.

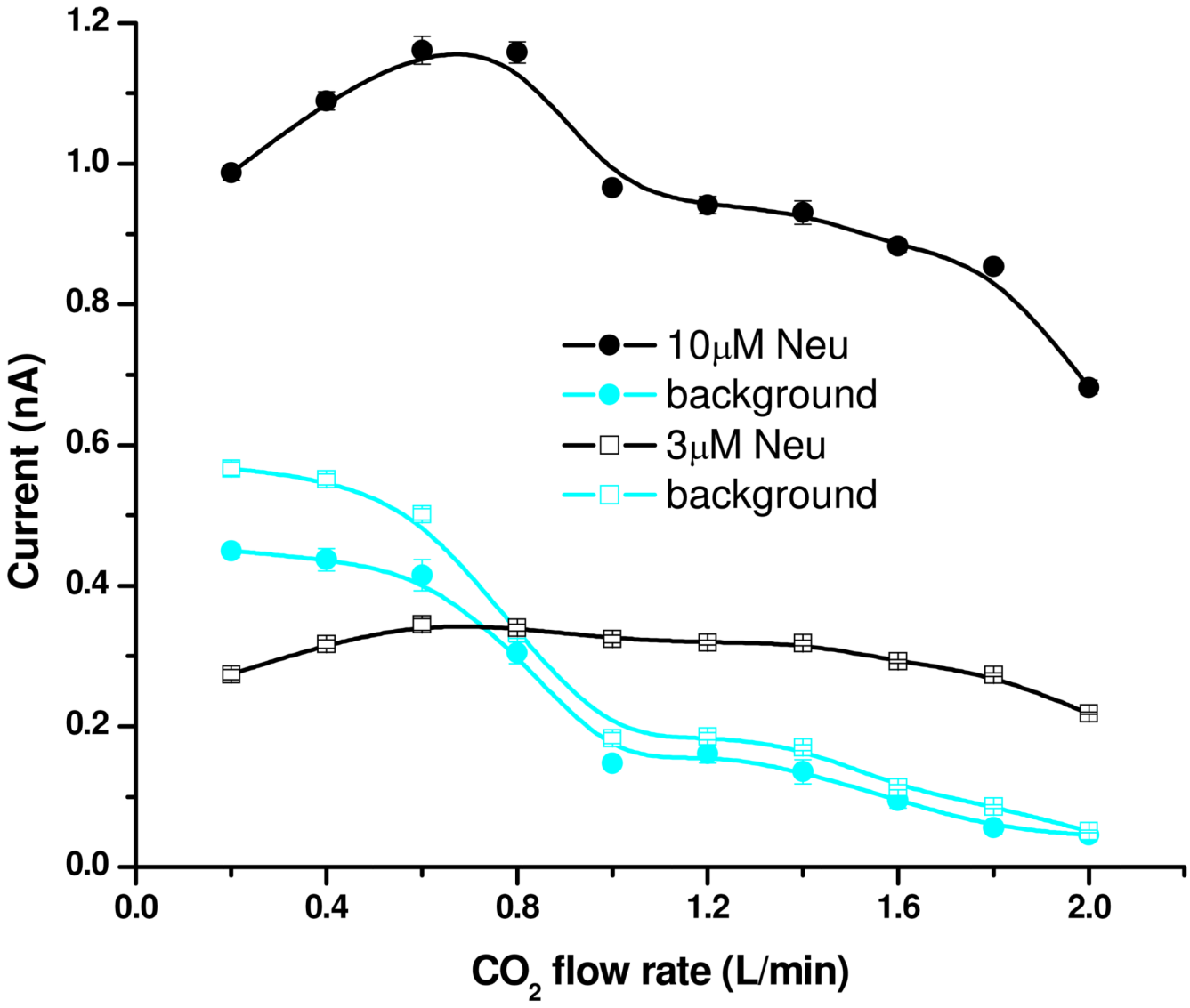

Figure 5.
Effect of concentration and CO_2 flow rate on current.

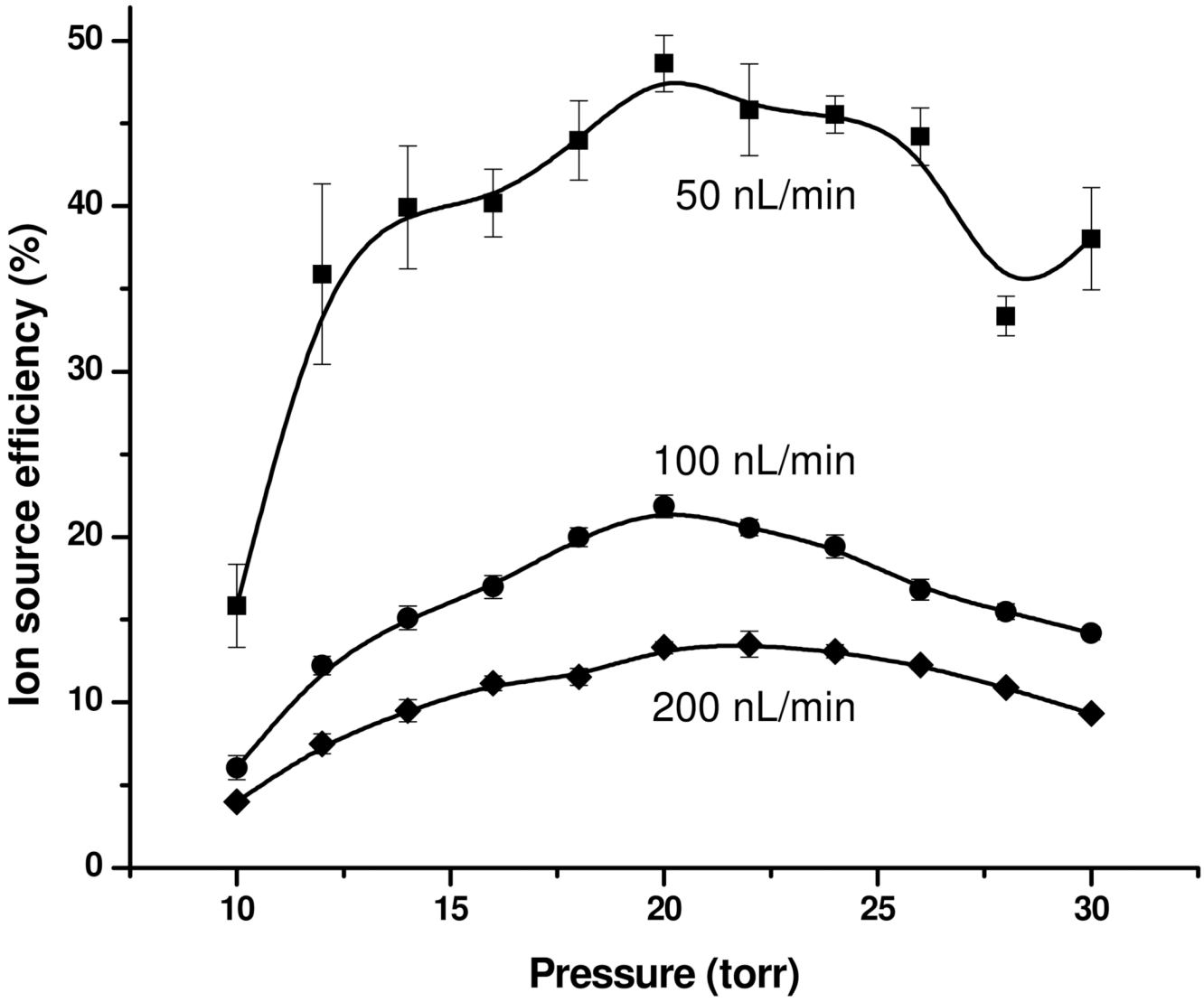

Figure 6.
Ion utilization efficiency as a function of pressure and liquid flow rate.